

# Chapter 4 The Cap Model and Its Implementation

---

## 4.1 Introduction

The "cap model falls within the framework of the classical incremental theory of work-hardening plasticity for materials that have time- and temperature-independent properties" (Chen and Baladi 1985). When modeling geologic materials subjected to stresses ranging from one to several hundred megapascals, the cap model has several desirable features. Of primary importance is its ability to model volumetric hysteresis through the use of a strain-hardening yield surface or cap.

In this chapter, the essential features of the cap model are reviewed, and the steps required to implement the cap model into the finite element code JAM are summarized. After a brief evaluation of the loading function and flow rule, the incremental elastic-plastic stress-strain relations are outlined. In addition, the cap model implemented into JAM is described, and the equations are developed for the elastic-plastic constitutive matrix and the plastic hardening modulus. Finally, the numerical implementation of the cap model itself is described. The reader should note that an engineering mechanics sign convention is used in which compression is negative.

## 4.2 Background

The cap model has been used by researchers in the ground shock community for approximately 20 years to simulate the responses of a wide variety of geologic materials. It is "predicated on the fact that the volumetric hysteresis exhibited by many geologic materials can also be described by a plasticity model, if the model is based on a hardening yield surface which includes conditions of hydrostatic stress" (Sandler et al. 1976). The model was first described in the open literature by DiMaggio and Sandler (1971). The FORTRAN source code for the model was published by Sandler and Rubin (1979).

As stated above, the cap model has several desirable features. Of primary importance is its ability to model volumetric hysteresis through the use of a strain-hardening yield surface or cap. The cap model may also be formulated with a nonlinear failure surface, with linear or nonlinear elastic moduli, or as a function of the third stress invariant. With the appropriate selection of material parameters, it can be used as a linear elastic or linear elastic-perfectly plastic material model. Sandler and Rubin (1979) demonstrated notable foresight with their use of function statements within the model, which allow substantial changes to be made to the cap model's potential functions with little programming effort.

Modifications and expansions of the original model were made by several researchers. Effective-stress versions of the cap model are reported in Baladi (1979), Baladi and Akers (1981), and Baladi and Rohani (1977, 1978, 1979). A transverse-isotropic cap was developed by Baladi (1978) and an elastic-viscoplastic cap model by Baladi and Rohani (1982). Rubin and Sandler (1977) developed a high-pressure cap model for ground shock calculations due to subsurface explosions. Baladi (1986) developed a "complex" strain-dependent cap model, which required 39 model parameters, for ground shock calculations of a dry cemented sand. In addition, several versions of the cap model are described in the text by Chen and Baladi (1985).

In formulating the cap model, DiMaggio and Sandler (1971) complied with the constraints imposed by Drucker's stability postulate. Drucker's stability postulate is sufficient, although not

necessary, to satisfy all thermodynamic and continuity requirements for continuum models (Sandler et al. 1976). Satisfying Drucker's stability postulate insures uniqueness, continuity, and stability of a solution and provides a mathematical problem that is properly posed. Rubin and Sandler (1977) state that "...the numerical solution to a properly posed problem can proceed without the fear that the results will be strongly dependent on errors of approximation of initial and boundary conditions, round off error, etc." Drucker (1951) defines a work-hardening material as one that remains in equilibrium under an added set of stresses applied by an external agency. It also means that "(a) positive work is done by the external agency during the application of the added set of stresses and (b) the net work performed by the external agency over the cycle of application and removal is positive if plastic deformation has occurred in the cycle" (Drucker 1951). Drucker (1950) states these two conditions in a mathematical format as

$$d\sigma_{ij} d\varepsilon_{ij} > 0 \quad \text{and} \quad \oint d\sigma_{ij} d\varepsilon_{ij}^p \geq 0$$

The first statement constrains a model such that strain-softening may not occur. The second statement implies (a) the loading function or yield surface must be convex and (b) the plastic strain increment vector must be normal to the yield surface, which means that an associated flow rule must be used. These are the constraints imposed by Drucker's stability postulate.

### 4.3 Loading Functions and Flow Rule

Drucker's criteria for stability permits considerable flexibility in the functional forms of the loading function  $f$ . Since Drucker's stability postulate requires the yield surface and plastic potential surface to coincide, the loading function  $f$  implicitly represents both the yield and potential surfaces. For a perfectly plastic material, a general form of the loading function may be written as

$$f(\sigma_{ij}) = 0 \tag{4.1}$$

and as

$$f(\sigma_{ij}, \kappa) = 0 \quad 4.2$$

for a strain- or work-hardening material, where  $\kappa$  is a hardening parameter that acts as an "internal state variable that measures hardening as a function of the history of plastic volumetric strain" (Sandler and Rubin 1979). For isotropic materials, the loading function may be expressed in terms of stress invariants, e.g.,

$$f(J_1, \sqrt{J_{2D}}, \kappa) = 0 \quad 4.3$$

where  $J_1 = \sigma_{kk}$  = the trace of the stress tensor and

$$J_{2D} = \frac{1}{2} s_{ij} s_{ij} = \text{the second invariant of the deviatoric stress tensor.}$$

This is the form of the loading function used in most versions of the cap model. The loading function is assumed to be isotropic and is comprised of two surfaces, an ultimate failure envelope and a strain-hardening surface or cap. The failure envelope, which is fixed in space and symmetric about the hydrostatic axis, limits the maximum shear stresses in the material and is expressed as

$$f = h(J_1, \sqrt{J_{2D}}) = \sqrt{J_{2D}} - Q(J_1) = 0 \quad 4.4$$

The cap, which moves as plastic deformations occur, is represented as

$$f = H(J_1, \sqrt{J_{2D}}, \kappa) = \sqrt{J_{2D}} - F(J_1, \kappa) = 0 \quad 4.5$$

The hardening parameter  $\kappa$  is generally taken to be a function of the plastic volume strain (Chen and Baladi 1985)

$$\kappa = g_1(\varepsilon_{kk}^p) \quad 4.6$$

Equation 4.6 allows the cap to expand and contract. By allowing the cap to contract, one can limit the amount of dilation that a material may develop when its stress path moves along the failure envelope  $h$ . This form of the hardening parameter is typically used for soil-like materials

that do not exhibit significant dilation during failure. For rock-like materials, the hardening parameter may be written as

$$\kappa = g_2 [ (\varepsilon_{kk}^p)_{\max} ] \quad 4.7$$

In this form, the cap is only permitted to expand, thus allowing a material to dilate while its stress path moves along the failure envelope, i.e., when  $h = 0$ . Both Equations 4.6 and 4.7 produce hysteresis during an imposed hydrostatic load-unload cycle (Baladi and Akers 1981).

The plastic loading criteria for the loading function  $f$  are given by

$$\frac{\partial f}{\partial \sigma_{ij}} d\sigma_{ij} \begin{cases} > 0 & \text{loading} \\ = 0 & \text{neutral loading} \\ < 0 & \text{unloading} \end{cases} \quad 4.8$$

(Baladi and Akers 1981). These criteria imply that during loading from a point on a given yield surface a stress increment tensor  $d\sigma_{ij}$  (when viewed as a vector) will point outward (Rohani 1977). Plastic strains will only occur under this condition. During unloading, the stress vector points inward, and the material will behave elastically. Neutral loading occurs when the stress vector is tangent to the yield surface. During neutral loading, no plastic strains are produced in the case of a work-hardening material (Rohani 1977). This is referred to as the "continuity condition", and its satisfaction leads to the coincidence of elastic and plastic constitutive equations (Chen and Baladi 1985).

Drucker (1951) has shown that the plastic strain increment tensor for a work-hardening material may be written as

$$d\varepsilon_{ij}^p = \begin{cases} d\lambda \frac{\partial f}{\partial \sigma_{ij}} & \text{if } f = 0 \text{ and } \frac{\partial f}{\partial \sigma_{ij}} d\sigma_{ij} > 0 \\ 0 & \text{if } f < 0, \text{ or } f = 0 \text{ and } \frac{\partial f}{\partial \sigma_{ij}} d\sigma_{ij} \leq 0 \end{cases} \quad 4.9$$

which is identical to the expression used for elastic-perfectly plastic materials. The term  $d\lambda$  is a positive factor of proportionality that is nonzero only when plastic deformations occur (Baladi and Akers 1981). For the cap model, the loading function  $f$  may take the form of either Equation 4.4 or 4.5.

#### 4.4 Derivation of Incremental Elastic-Plastic Stress-Strain Relations

The basic premise in the formulation of the cap model and all elastic-plastic constitutive models is that certain materials are capable of undergoing small plastic (permanent) strains as well as small elastic (recoverable) strains during each loading increment (Baladi and Akers 1981). This may be expressed mathematically as

$$d\varepsilon_{ij} = d\varepsilon_{ij}^e + d\varepsilon_{ij}^p \quad 4.10$$

where  $d\varepsilon_{ij}$  = components of the total strain increment tensor,

$d\varepsilon_{ij}^e$  = components of the elastic strain increment tensor, and

$d\varepsilon_{ij}^p$  = components of the plastic strain increment tensor.

This equation simply states that the total strain increment is equal to the sum of the elastic and plastic strain increments. In its most general form, the elastic strain increment tensor may be expressed as

$$d\varepsilon_{ij}^e = C_{ijkl} d\sigma_{kl} \quad 4.11$$

where  $C_{ijkl}(\sigma_{mn})$  = the material response function, which may be a function of stress.

For isotropic materials, the elastic strain increment tensor may be expressed as

$$d\varepsilon_{ij}^e = \frac{dJ_1}{9K} \delta_{ij} + \frac{ds_{ij}}{2G} \quad 4.12$$

where  $s_{ij} = \sigma_{ij} - (J_1/3) \delta_{ij}$  = the deviatoric stress tensor,

$\delta_{ij}$  = the Kronecker delta, and

$K$  and  $G$  are the elastic bulk and shear moduli, respectively.

The elastic bulk and shear moduli may be constants or functions of stress or strain invariants, e.g.,

$$\begin{aligned} K &= K(J_1, J_{2D}, J_{3D}) \\ G &= G(J_1, J_{2D}, J_{3D}) \end{aligned} \quad 4.13$$

where  $J_{3D} = 1/3 s_{ij} s_{jk} s_{ki}$  = the third invariant of the deviatoric stress tensor.

Chen and Baladi (1985) discuss the thermodynamic restrictions to the possible forms of the above equations. Permissible functional forms of  $K$  and  $G$  must not generate energy or hysteresis and must maintain the path-independent behavior of elastic materials. Thus, the bulk and shear moduli should be limited to the following forms (Chen and Baladi 1985)

$$\begin{aligned} K &= K(J_1, \varepsilon_{ij}^p) \\ G &= G(J_{2D}, \varepsilon_{ij}^p) \end{aligned} \quad 4.14$$

Inclusion of the plastic strain tensor into the functional forms of  $K$  and  $G$  is permitted since plastic strains are constant during periods of elastic deformation. Under these restrictions, the hydrostatic and deviatoric components of the elastic strain increment tensor (Equation 4.12) may be written as

$$d\varepsilon_{kk}^e = \frac{dJ_1}{3K(J_1, \varepsilon_{ij}^p)} \quad 4.15$$

and

$$de_{ij}^e = \frac{ds_{ij}}{2G(J_{2D}, \varepsilon_{ij}^p)} \quad 4.16$$

Combining Equations 4.9 and 4.12, the total strain increment tensor can be written as

$$d\varepsilon_{ij} = \frac{dJ_1}{9K} \delta_{ij} + \frac{ds_{ij}}{2G} + d\lambda \frac{\partial f}{\partial \sigma_{ij}} \quad 4.17$$

The plastic strain increment tensor (Equation 4.9) may also be expressed in terms of the hydrostatic and deviatoric components of strain. Applying the chain rule of differentiation to the right-hand side of Equation 4.9 results in

$$d\varepsilon_{ij}^p = d\lambda \left( \frac{\partial f}{\partial J_1} \frac{\partial J_1}{\partial \sigma_{ij}} + \frac{\partial f}{\partial \sqrt{J_{2D}}} \frac{\partial \sqrt{J_{2D}}}{\partial \sigma_{ij}} \right) \quad 4.18$$

which simplifies to

$$d\varepsilon_{ij}^p = d\lambda \left( \frac{\partial f}{\partial J_1} \delta_{ij} + \frac{1}{2\sqrt{J_{2D}}} \frac{\partial f}{\partial \sqrt{J_{2D}}} s_{ij} \right) \quad 4.19$$

Multiplying both sides of Equation 4.19 by  $\delta_{ij}$  gives an expression for the plastic volumetric strain

$$de_{kk}^p = 3 d\lambda \frac{\partial f}{\partial J_1} \quad 4.20$$

By definition, the deviatoric component of the plastic strain increment tensor is written as

$$de_{ij}^p = d\varepsilon_{ij}^p - \frac{1}{3} de_{kk}^p \delta_{ij} \quad 4.21$$

Substitution of Equations 4.19 and 4.20 into Equation 4.21 gives

$$de_{ij}^p = \frac{d\lambda}{2\sqrt{J_{2D}}} \frac{\partial f}{\partial \sqrt{J_{2D}}} s_{ij} = d\lambda \frac{\partial f}{\partial s_{ij}} \quad 4.22$$

The proportionality factor  $d\lambda$  must be determined prior to evaluating any of the above plastic strains. Baladi and Akers(1981), Chen and Baladi(1985), and Rohani(1977) outline the methods required to evaluate the proportionality factor. Those methods are documented in Appendix D.

## 4.5 Elastic-Plastic Constitutive Matrix

In the following section, the equations for the elastic-plastic constitutive matrix are formulated. The equations are written in matrix format to render a more compact form of the equations. The development of the elastic-plastic constitutive matrix follows the derivation of Owen and Hinton (1980).

The loading or yield function  $f$  for a general work- or strain-hardening elastic-plastic model (Equation 4.2) may be rewritten as:

$$f(\boldsymbol{\sigma}, \kappa) = F(\boldsymbol{\sigma}) - k(\kappa) = 0 \quad 4.23$$

where (in matrix format)  $\boldsymbol{\sigma}$  is the vector of normal and shear stresses and  $\kappa$  is the hardening parameter that controls the expansion of the yield surface. Recall that in the cap model, the cap itself is the only strain-hardening yield surface; the failure envelope is not a hardening surface. Equation 4.23 may be differentiated to give:

$$df = \frac{\partial f}{\partial \boldsymbol{\sigma}} d\boldsymbol{\sigma} + \frac{\partial f}{\partial \kappa} d\kappa = 0 \quad 4.24$$

or in another form:

$$\mathbf{a}^T d\boldsymbol{\sigma} - A d\lambda = 0 \quad 4.25$$

where

$$\mathbf{a}^T = \frac{\partial f}{\partial \boldsymbol{\sigma}} = \frac{\partial f}{\partial \sigma_{ij}} \quad 4.26$$

and

$$A = -\frac{1}{d\lambda} \frac{\partial f}{\partial \kappa} d\kappa \quad 4.27$$

Owen and Hinton refer to the vector  $\mathbf{a}$  as the *flow vector*. The scalar  $A$  will be identified as the plastic hardening modulus.

The total strain increment tensor (Equation 4.10) may be written in matrix format as

$$d\boldsymbol{\varepsilon} = d\boldsymbol{\varepsilon}^e + d\boldsymbol{\varepsilon}^p \quad 4.28$$

By substituting for both the elastic and plastic strain increments, i.e., using the matrix equivalents of Equations 4.9 and 4.11, the following expression is obtained:

$$d\boldsymbol{\varepsilon} = \mathbf{D}^{-1} d\boldsymbol{\sigma} + d\lambda \frac{\partial f}{\partial \boldsymbol{\sigma}} \quad 4.29$$

where  $\mathbf{D}$  is the matrix of elastic material constants and the inverse of the material response function. After multiplying Equation 4.29 by  $\mathbf{a}^T \mathbf{D}$  one obtains:

$$\mathbf{a}^T \mathbf{D} d\boldsymbol{\varepsilon} = \mathbf{a}^T d\boldsymbol{\sigma} + \mathbf{a}^T \mathbf{D} \mathbf{a} d\lambda \quad 4.30$$

which may be refined further by eliminating  $\mathbf{a}^T d\boldsymbol{\sigma}$  with the use of Equation 4.25 to produce:

$$\mathbf{a}^T \mathbf{D} d\boldsymbol{\varepsilon} = \left[ A + \mathbf{a}^T \mathbf{D} \mathbf{a} \right] d\lambda \quad 4.31$$

This leads to an expression for the scalar term  $d\lambda$ :

$$d\lambda = \frac{\mathbf{a}^T \mathbf{D} d\boldsymbol{\varepsilon}}{\left[ A + \mathbf{a}^T \mathbf{D} \mathbf{a} \right]} \quad 4.32$$

This term gives the magnitude of the plastic strain increment vector and is the matrix form of Equation D.5. Note that in the text by Owen and Hinton (1980), this expression was printed incorrectly.

Having defined an expression for  $d\lambda$ , it may be substituted into Equation 4.29 to give:

$$\mathbf{D}^{-1} d\boldsymbol{\sigma} = \left\{ 1 - \frac{\mathbf{d}_D^T \mathbf{a}}{[A + \mathbf{d}_D^T \mathbf{a}]} \right\} d\boldsymbol{\varepsilon} \quad 4.33$$

where  $\mathbf{d}_D^T = \mathbf{a}^T \mathbf{D}$ .

Multiplying both sides of Equation 4.33 by  $\mathbf{D}$  gives:

$$d\boldsymbol{\sigma} = \left\{ \mathbf{D} - \frac{\mathbf{D} \mathbf{a} \mathbf{d}_D^T}{[A + \mathbf{d}_D^T \mathbf{a}]} \right\} d\boldsymbol{\varepsilon} \quad 4.34$$

which is an expression for the elastic-plastic incremental stress-strain relation. If we substitute  $\mathbf{d}_D = \mathbf{D} \mathbf{a}$ , then the elastic-plastic constitutive matrix may be expressed as:

$$\mathbf{D}^{ep} = \left\{ \mathbf{D} - \frac{\mathbf{d}_D \mathbf{d}_D^T}{[A + \mathbf{d}_D^T \mathbf{a}]} \right\} \quad 4.35$$

## 4.6 Plastic Hardening Modulus

The plastic hardening modulus  $A$  must now be evaluated for a strain-hardening formulation such as the cap model. If the hardening parameter  $\kappa$  is a function of the plastic strains, i.e.,

$$\kappa = g(\boldsymbol{\varepsilon}^p) \quad 4.36$$

then Equation 4.36 may be differentiated to give:

$$d\kappa = \frac{\partial \kappa}{\partial \boldsymbol{\varepsilon}^p} d\boldsymbol{\varepsilon}^p \quad 4.37$$

Substituting Equation 4.37 into Equation 4.27, substituting for  $\boldsymbol{\varepsilon}^p$ , and rearranging produces:

$$A = -\frac{\partial f}{\partial \kappa} \frac{\partial \kappa}{\partial \boldsymbol{\varepsilon}^p} \frac{\partial f}{\partial \boldsymbol{\sigma}} \quad 4.38$$

The plastic hardening modulus  $A$  will be dependent upon the functional form of the loading or yield function  $f$  and the hardening function used in the cap model.

## 4.7 Cap Model Implemented into JAM

The following section describes the version of the cap model implemented into the finite element code JAM. The functional forms of the equations are outlined, and the cap model is described in more detail.

Two elastic response functions govern the behavior of the model in the elastic regime. The elastic bulk modulus is defined by the following equation

$$K(J_1, \varepsilon_{kk}^p) = \frac{K_i}{1 - K_1} \left[ 1 - K_1 \exp(K_2 \varepsilon_{kk}^p) \right] \quad 4.39$$

where  $K_i$  = the initial elastic bulk modulus and

$K_1$  and  $K_2$  are material constants.

The elastic bulk modulus prescribes the unloading moduli in pressure-volume space. The three material constants may be determined from the unloading data obtained during hydrostatic loading tests. The elastic shear modulus is defined by the following equation

$$G(J_{2D}, \varepsilon_{kk}^p) = \frac{G_i}{1 - G_1} \left[ 1 - G_1 \exp(G_2 \varepsilon_{kk}^p) \right] \quad 4.40$$

where  $G_i$  = the initial elastic shear modulus and

$G_1$  and  $G_2$  are material constants.

The elastic shear modulus prescribes the unloading moduli in principal stress difference-principal strain difference space. The three material constants may be determined from the unloading shear data of triaxial compression tests. The constants for the elastic bulk and shear moduli may also be determined from uniaxial strain compression tests, i.e., from the unloading slopes of the stress path ( $= 2G/K$ ) and stress-strain curves ( $= K + 4/3 G$ ).

In the current model, the failure envelope portion of the loading function  $f$  is defined by a modified Drucker-Prager failure surface (see Figure 4.1) of the form

$$h(J_1, \sqrt{J_{2D}}) = \sqrt{J_{2D}} - [A - C \exp(B J_1)] \quad \text{if } J_1 > L(\kappa) \quad 4.41$$

where  $A$ ,  $B$  and  $C$  are material constants. These constants may be determined from the locus of triaxial compression failure data plotted in the appropriate stress space. The strain-hardening yield surface or cap is described by the following

$$H(J_1, \sqrt{J_{2D}}, \kappa) = \sqrt{J_{2D}} - \frac{1}{R} \left\{ [X(\kappa) - L(\kappa)]^2 - [J_1 - L(\kappa)]^2 \right\}^{0.5} \quad \text{if } J_1 < L(\kappa) \quad 4.42$$

where  $X(\kappa)$  and  $L(\kappa)$  define the values of  $J_1$  at the intersection of the cap with the  $J_1$  axis and at the center of the cap, respectively (see Figure 4.1);  $\kappa$  is the hardening parameter, which is equal to the plastic volumetric strain, i.e.,

$$\kappa = \varepsilon_{kk}^p \quad 4.43$$

The value of  $J_1$  determines which of the two yield surfaces should be used, as indicated by Equations 4.41 and 4.42.  $R$  is the ratio of the major to minor axes of the elliptical cap and has the following functional form

$$R[L(\kappa)] = R_i + R_1 \left[ 1 - \exp\left(R_2 \{L(\kappa) - L_0\}\right) \right] \quad 4.44$$

where  $R_i, R_1, R_2$  and  $L_0$  are material constants;  $L_0$  defines the initial location of the cap.

Chen and Baladi (1985) explain that the functional form of the cap was chosen such that the tangent of its intersection with the failure envelope is horizontal. This condition is guaranteed by the following relationship between  $X(\kappa)$  and  $L(\kappa)$

$$X(\kappa) = L(\kappa) - R h(l(\kappa), \sqrt{J_{2D}}) \quad 4.45$$

where

$$L(\kappa) = \begin{cases} l(\kappa) & \text{if } l(\kappa) < 0 \\ 0 & \text{if } l(\kappa) \geq 0 \end{cases} \quad 4.46$$

The hardening function for this model is defined by

$$\varepsilon_{kk}^p = W \left( e^{[D(X(\kappa) - X_0)]} - 1 \right) \quad 4.47$$

which may be rewritten in the following form

$$X(\kappa) = \frac{1}{D} \ln \left( \frac{\varepsilon_{kk}^p}{W} + 1 \right) + X_0 \quad 4.48$$

where  $D, W$  and  $X_0$  are material constants.  $W$  establishes the maximum plastic volumetric strain the material can develop;  $X_0$ , like  $L_0$ , defines the initial location of the cap.

As described previously, Drucker's stability postulate places limits on the functional forms of the equations in the cap model. Sandler and Rubin (1979) specify some of those limitations: (a)  $Q(J_1)$  must decrease monotonically with increasing values of  $J_1$ ; (b) to avoid work-softening, the functions  $X(\kappa)$  and  $L(\kappa)$  must be continuous and monotonically increasing functions and

$$\frac{\partial F}{\partial J_1} \geq 0 \quad \text{and} \quad \frac{\partial F}{\partial \kappa} < 0$$

(c) the cap must extend from the  $J_1$  axis to a point on or below the failure envelope  $h$ , i.e.,

$$F [ X(\kappa), \kappa ] = 0 \quad 4.49$$

and

$$F [ L(\kappa), \kappa ] \leq Q [ L(\kappa) ] \quad 4.50$$

(d) within the yield surfaces defined by

$$\sqrt{J_{2D}} < Q(J_1) \quad \text{for } J_1 > L(\kappa) \quad 4.51$$

and

$$\sqrt{J_{2D}} < F(J_1, \kappa) \quad \text{for } L(\kappa) \geq J_1 \geq X(\kappa) \quad 4.52$$

the material response must be isotropic elastic. Sandler and Rubin (1979) explain that if the inequality in Equation 4.50 is true, then a gap exists between the cap  $H$  and the failure envelope  $h$  and a von Mises type failure surface is used as a transition between the two yield surfaces (Figure 4.1). The yield surface for  $J_1 \geq L(\kappa)$  is thus defined by the following expression

$$\sqrt{J_{2D}} \equiv \min \{ F [ L(\kappa), \kappa ] , Q [ J_1 ] \} \quad 4.53$$

In the evaluation of plastic hardening modulus  $A$ , one need only be concerned with the functional form of the cap since it is the only hardening surface in the model. In order to evaluate  $A$ , each of the three terms in Equation 4.38 must be evaluated. Recalling Equation 4.43, the first term may be expanded as

$$\frac{\partial H}{\partial \kappa} = \frac{\partial H}{\partial X} \frac{\partial X}{\partial \kappa} = \frac{\partial H}{\partial X} \frac{\partial X}{\partial \varepsilon_{kk}^p} \quad 4.54$$

Each of these terms is evaluated as

$$\frac{\partial X}{\partial \varepsilon_{kk}^p} = \frac{1}{D(\varepsilon_{kk}^p + W)} \quad 4.55$$

and

$$\frac{\partial H}{\partial X} = 2(L - X) \quad 4.56$$

Combining the terms gives

$$\frac{\partial H}{\partial \kappa} = \frac{2(L - X)}{D(\varepsilon_{kk}^p + W)} \quad 4.57$$

The second term in the expression for  $A$  is evaluated as

$$\frac{\partial \kappa}{\partial \varepsilon_{ij}^p} = \delta_{ij} \quad 4.58$$

since  $\kappa = \varepsilon_{kk}^p$ . The final term in  $A$  can be expanded as

$$\frac{\partial H}{\partial \sigma_{ij}} = \frac{\partial H}{\partial J_1} \delta_{ij} + \frac{s_{ij}}{2\sqrt{J_{2D}}} \frac{\partial H}{\partial \sqrt{J_{2D}}} \quad 4.59$$

Recalling that  $s_{ij} \delta_{ij} = 0$  and substituting Equations 4.57-4.59 into Equation 4.38, one gets

$$A = \frac{6(X - L)}{D(\varepsilon_{kk}^p + W)} \frac{\partial H}{\partial J_1} \quad 4.60$$

as an expression for  $A$ . Simplifying this further by evaluating

$$\frac{\partial H}{\partial J_1} = 2(J_1 - L) \quad 4.61$$

and substituting into Equation 4.60, one obtains the final expression for the plastic hardening modulus

$$A = \frac{12(X - L)(J_1 - L)}{D(\varepsilon_{kk}^p + W)} \quad 4.62$$

The details of the numerical implementation of the cap model itself are documented in Appendix E.

## 4.8 Implementation of Cap Model into JAM

Two basic operations that are associated with elastic-plastic material models must be performed in most implicit finite element codes: (1) the construction of the elastic-plastic constitutive matrix and (2) the calculation of the residual forces. The purpose of this section is to explain how these two operations were affected by the implementation of the cap model. The later operation will be considered first since it is a straight forward process.

After the strain increments at time  $t + \Delta t$  are obtained from the solution of the field equations, the stresses at time  $t + \Delta t$  in each element are calculated. The residual forces at time  $t + \Delta t$  are then calculated based on the stress states in the elements. In this operation, no substantial changes are required in the cap model subroutines; hence, the implementation is rather simple.

However, three components, the elastic constitutive matrix  $D$ , the plastic hardening modulus  $A$ , and the flow vector  $a$ , are required to calculate the elastic-plastic constitutive matrix  $D^{ep}$ . The calculation of the elastic constitutive matrix is simple and needs no further discussion. In JAM, a modified cap-model subroutine calculates and returns values for the flow vector and the plastic hardening modulus. This subroutine first determines which of four possible regions or surfaces a stress point resides in or on, i.e., an elastic region, the failure surface, the cap, or the

tension cutoff. The plastic hardening modulus is nonzero only when the stress point falls on the cap since it is the only hardening surface. In this case, the plastic hardening modulus is calculated using Equation 4.62. The flow vector is calculated by numerically evaluating Equation 4.59 when the stress state lies on the failure surface, the cap, or the tension cutoff.

To complete the implementation, one must provide the model access to the material constants and an array to store the location of the cap for each numerical integration point.

## 4.9 Verification

To insure that the cap model was correctly incorporated into the finite element program JAM, several laboratory stress- and strain-path tests were numerically simulated. These calculations were compared to the output from a cap model driver (Chen and Baladi 1985) exercised over the same laboratory stress and strain paths. The two programs should produce similar if not identical results. The cap model constants used in these verification calculations are listed in Table 4.1

The following tests and strain paths were simulated: a hydrostatic compression test with one load/unload cycle, a set of constant radial stress triaxial compression tests, a set of constant mean normal stress tests, a uniaxial strain ( $K_0$ ) test with one load/unload cycle, and finally a test with a  $K_0$  load/constant axial strain (BX) unload cycle. To simulate the tests with the finite element program, a single element was loaded under the

**Table 4.1.**  
**Cap Model Constants for Verification Problems**

Cap model parameters		
Parameter	Value	Units
A	5017.32	MPa
C	5000	MPa
B	0.0142E-3	1/MPa
$K_i$	29800	MPa
$K_1$	0.	--
$K_2$	0.	--
$G_i$	11425	MPa
$G_1$	0.	--
$G_2$	0.	--
$R_i$	3.0	--
$R_1$	0.	--
$R_2$	0.	--
W	0.235	--
D	0.008	1/MPa
$X_0$	0.	MPa

appropriate boundary conditions. Several loading increments were utilized during each calculation, and a convergence tolerance of 1 percent was satisfied at the end of each increment. The output at the end of each increment is represented by a symbol on the comparison plots.

The simulated hydrostatic loading test consisted of an applied loading to a pressure level of 250 MPa, followed by an unloading to zero pressure. This calculation exercised the logic and code affecting both the cap movements and the elastic algorithms within the model and finite element program. The finite element and cap model driver results are compared in [Figure 4.2](#). Output from the finite element program matches the cap model driver with no noticeable errors.

Four constant radial stress triaxial compression tests at radial stresses of 25, 50, 100, and 150 MPa were simulated. Loading was terminated prior to reaching the ultimate failure surface, and unloading results were acquired for only three of the four calculations. The values of principal stress difference calculated by the finite element program were less than those of the cap model driver ([Figure 4.3](#)). The magnitude of the errors decreased when a larger number of increments was applied.

Four constant mean normal stress tests at confining pressures of 25, 50, 100, and 150 MPa were simulated. As with the simulated triaxial compression tests, loading was terminated prior to reaching the ultimate failure surface; unloading results were not acquired. The finite element and cap model driver results are compared in [Figure 4.4](#). Errors in the stresses calculated by the finite element program were less than those in the simulated triaxial compression tests ([Figure 4.3](#)).

The simulated  $K_0$  test consisted of an applied loading to a vertical strain level of 20 percent, followed by an unloading to a small value of vertical stress. In this calculation, the finite element simulation was conducted with a displacement controlled boundary condition. This type of loading should produce an exact match between the finite element program and the cap model driver since no strain increment iterations are required in the finite element program. The

calculated  $K_0$  stress-strain response is plotted in [Figure 4.5](#) and the stress path response in [Figure 4.6](#). There are no noticeable differences between the two calculations.

A  $K_0$  load/BX unload test was also simulated with a displacement controlled boundary condition. The test consisted of an applied loading to 20 percent axial strain, followed by an unloading to a small value of radial stress ([Figure 4.7](#)). In this calculation, the corner coding of the cap model was exercised as the stress path unloaded along the failure envelope ([Figure 4.8](#)). The calculated results suggest a proper implementation of this logic.

## 4.10 Summary

The features of the cap model and the relevant equations were documented in this chapter. In addition, the steps required to implement the cap model into the FE code were summarized. The implementation of the cap model was verified by comparing the output from the FE code and a driver for the cap model.

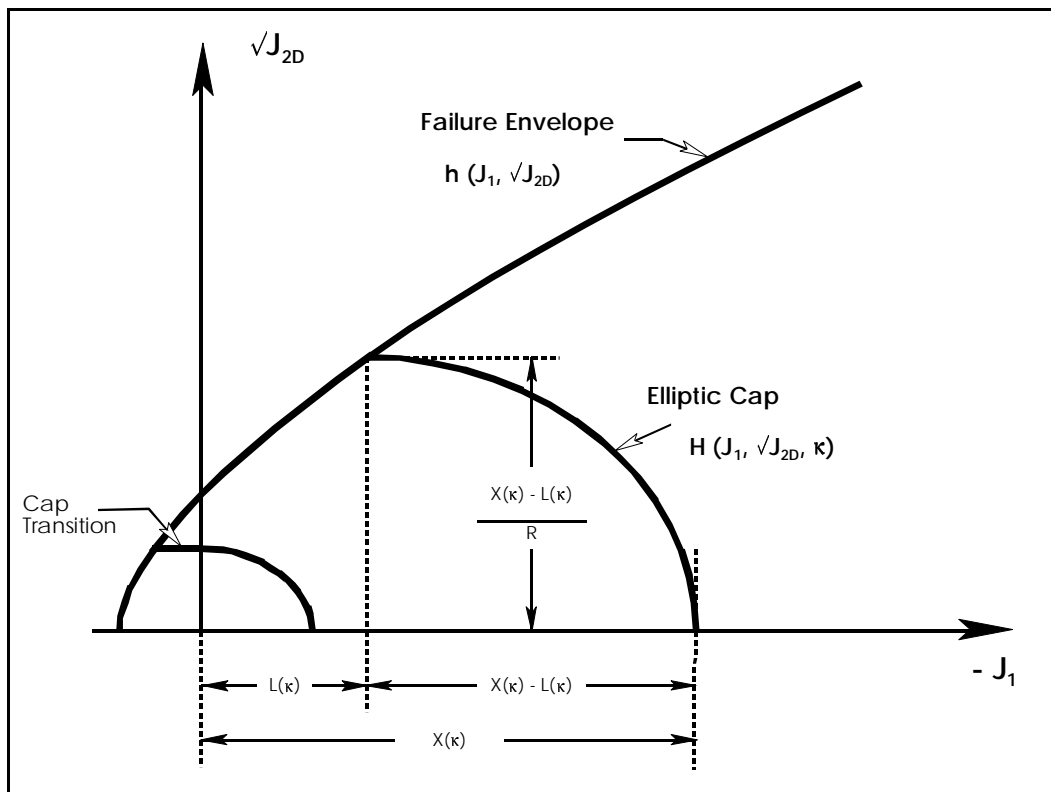


Figure 4.1. Cap model yield surfaces

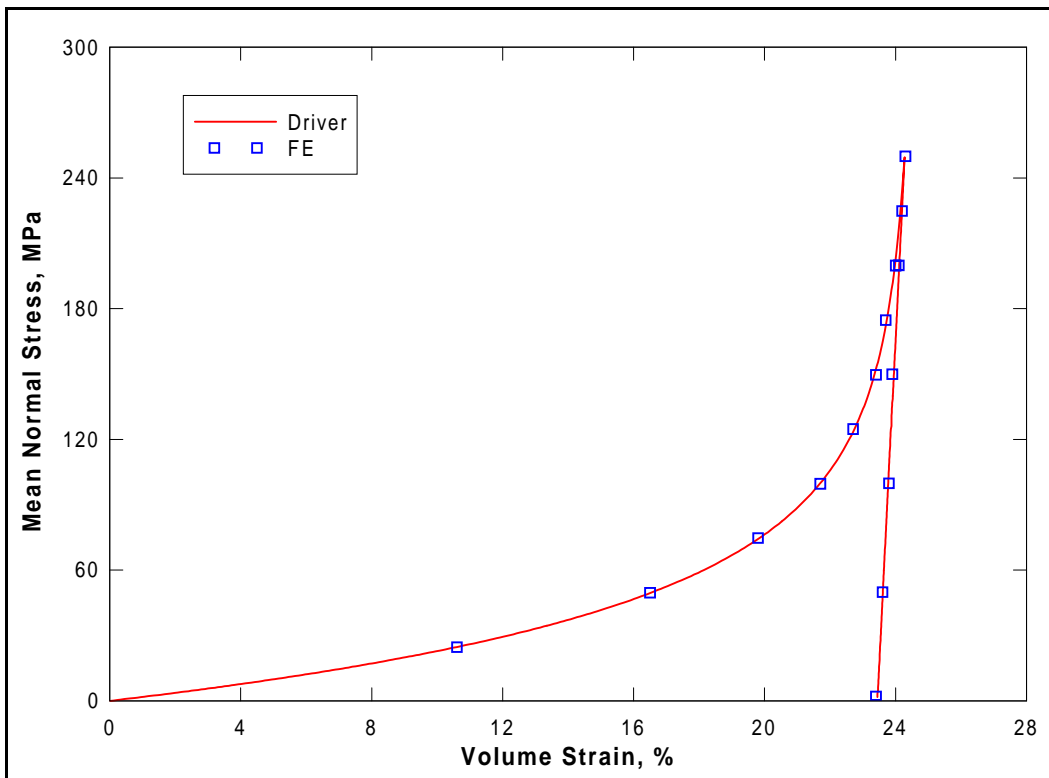


Figure 4.2. Simulated hydrostatic loading stress-strain response

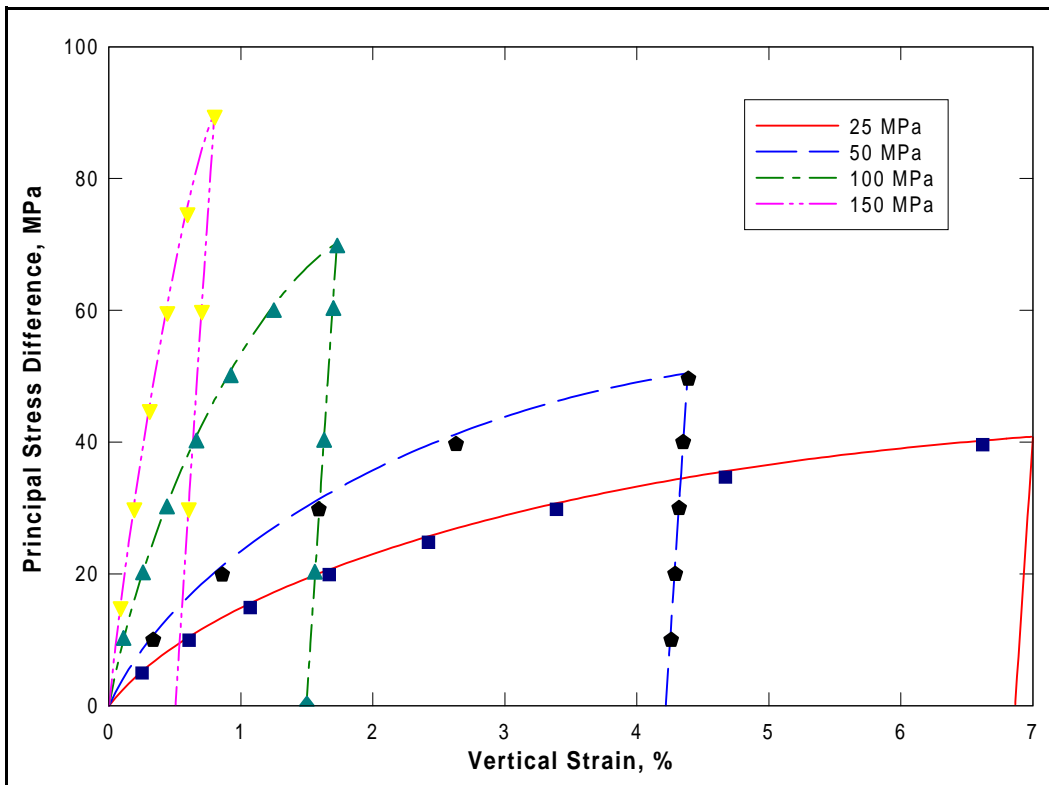


Figure 4.3. Simulated triaxial compression stress-strain response

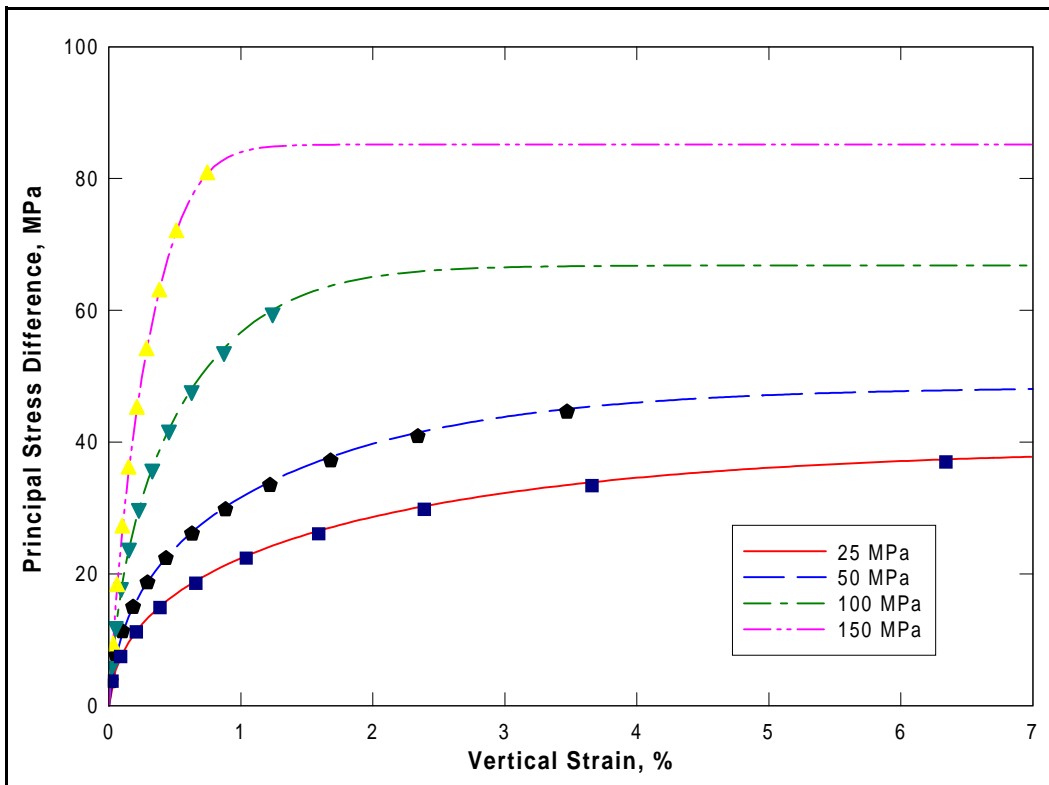


Figure 4.4. Simulated stress-strain response of constant mean normal stress tests

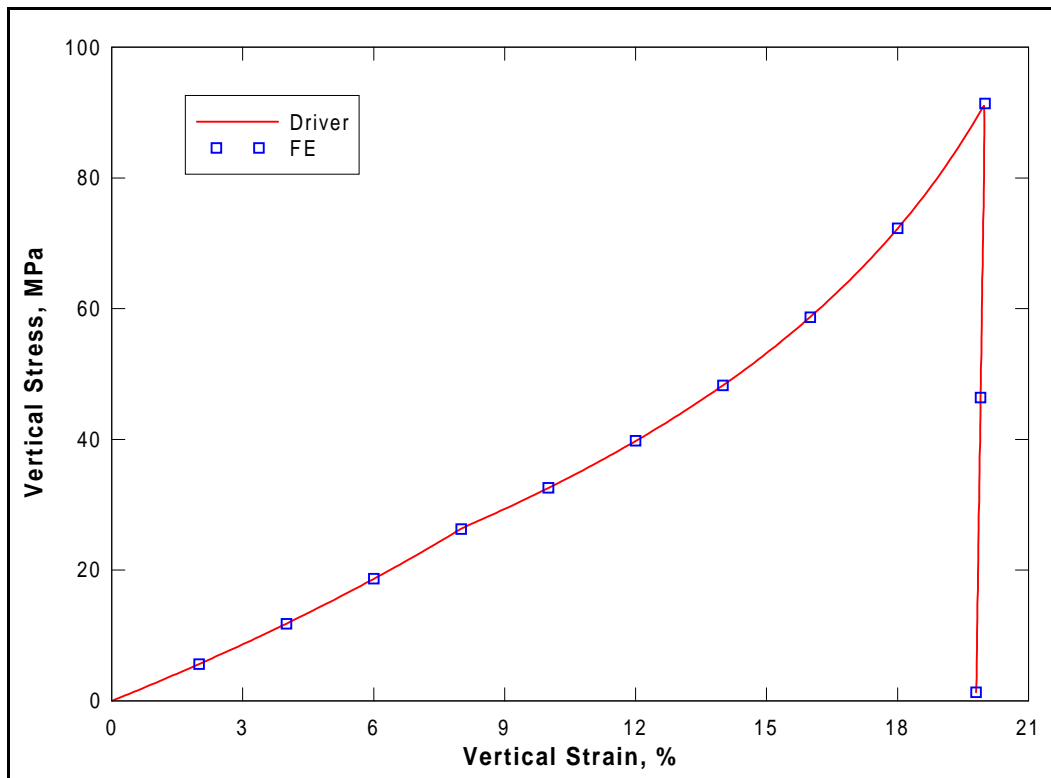


Figure 4.5. Stress-strain response of simulated UX test

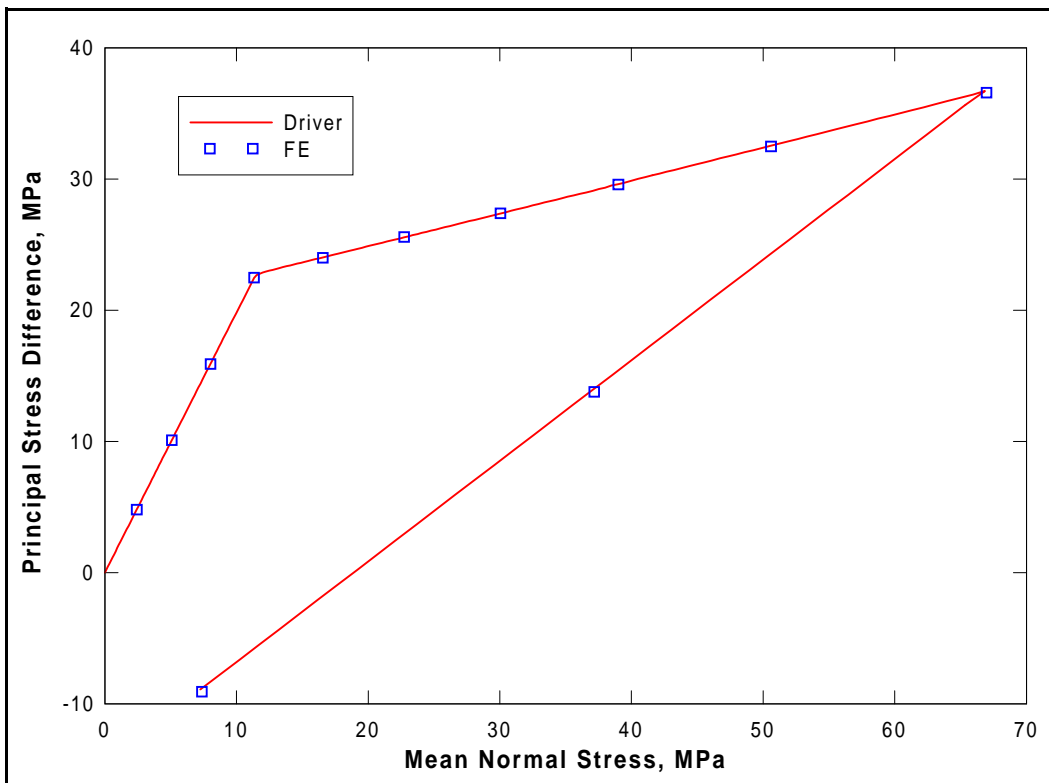


Figure 4.6. Stress path from simulated UX test

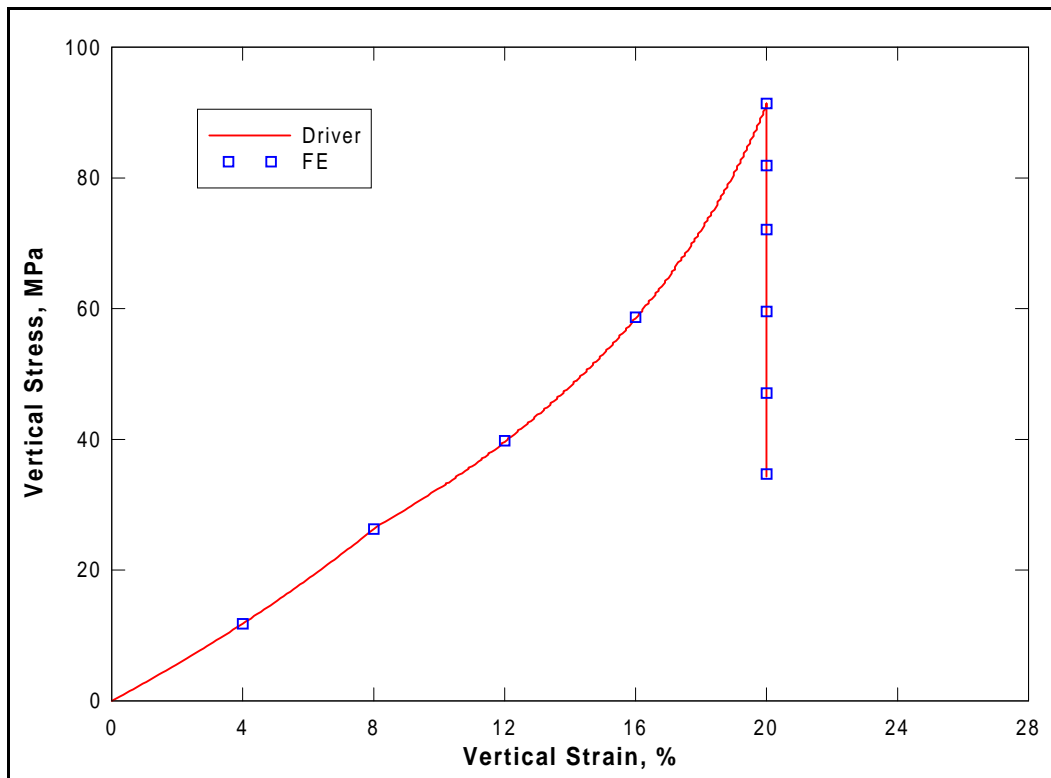


Figure 4.7. Stress-strain response of simulated UX/BX test

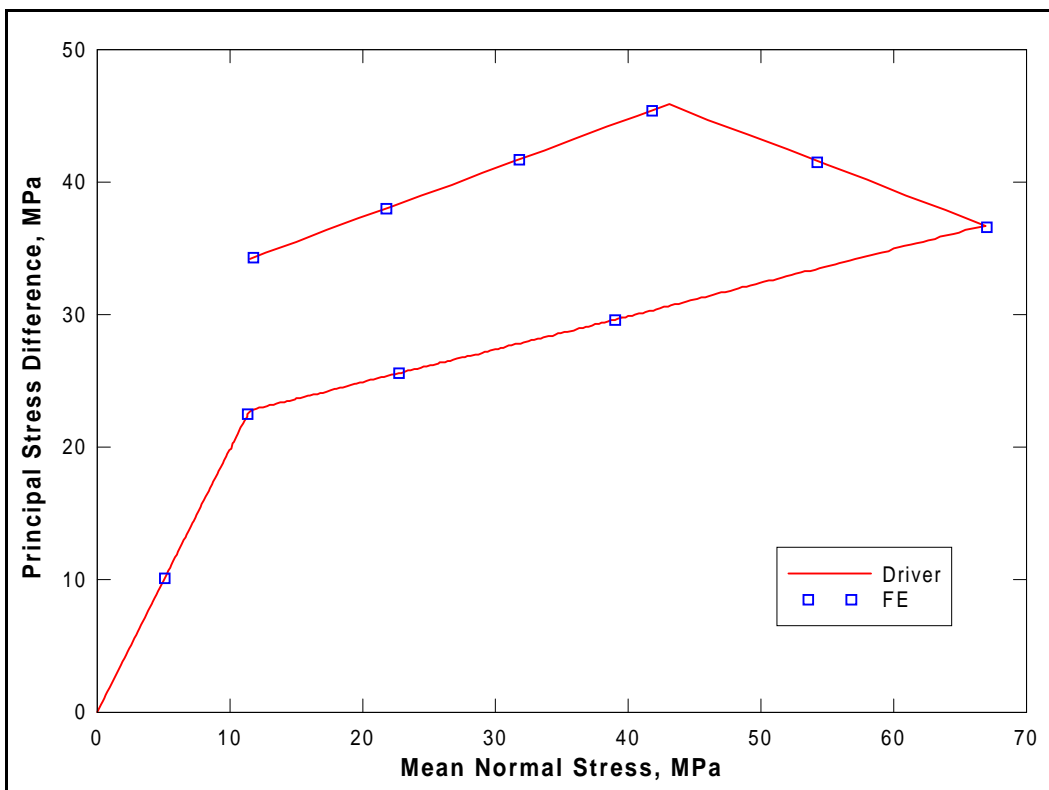


Figure 4.8. Stress path from simulated UX/BX test